PHYSICAL REVIEW B VOLUME 60, NUMBER 8 15 AUGUST 1999-II

$k_{\parallel}=0$ filtering in resonant-tunneling processes between materials of different effective electron mass

J. Smoliner,* R. Heer, and G. Strasser
Institut für Festkörperelektronik and Mikrostrukturzentrum der TU-Wien, Floragasse 7, A-1040 Wien, Austria
(Received 18 May 1999)

If electrons are transferred across an interface between an area of high and low effective mass, parallel momentum conservation leads to electron refraction effects, which are evident on InAs-AlSb resonant tunneling diodes and also, e.g., in ballistic electron emission microscopy. In ballistic electron emission microscopy on Au-GaAs Schottky diodes, the difference in effective mass is especially large and as a consequence of electron refraction, the spatial and energetic resolution for structures buried below the metal-semiconductor interface are considerably reduced. If a resonant (GaAs-$Al_xGa_{1-x}As$) tunneling structure is grown directly below the sample surface, however, only electrons with zero wave vector parallel to the barriers can be transmitted resonantly. As a consequence, the energetic and spatial resolution is expected to be enhanced for buried structures. Moreover, the underlying principle can be applied to devices in order to fabricate electron injector structures with narrow energy distribution both in $E_{\perp}$ and $E_{\parallel}$. [S0163-1829(99)50232-4]

Until now, only little attention has been paid to the physical effects that occur when electrons are transferred between areas of different effective mass. In double barrier resonant-tunneling diodes based on the InAs-AlSb material system, however, effective mass effects had to be taken into account,[1] since the difference in effective mass between both material systems is quite large. On these samples it was found that the current voltage characteristics differ qualitatively from the theoretically calculated curves, which is due to a coupling between the longitudinal and transversal components of the wave vectors in tunneling processes between areas of different effective mass.[2,3] In the following, such tunneling processes were studied in more detail. Both the influence of a position dependent mass and the angular dependence of the transmission coefficient were investigated[4] and most recently, a spatially varying effective mass was incorporated into the original Tsu-Esaki model.[3,5]

A second field of research, where electrons are transferred between regions of different effective mass, is ballistic electron emission microscopy (BEEM).[6,7] BEEM is a three terminal extension of conventional scanning tunneling microscopy (STM), where ballistic electrons are injected from a STM tip into a semiconductor via a thin metal base layer evaporated onto the sample. The corresponding ballistic electron current as a function of sample bias is called BEEM spectrum and is measured via a collector contact.

Originally, BEEM was mostly applied to study semiconductor interface properties such as metal-semiconductor Schottky barrier heights.[8–11] Later, BEEM experiments were also used to study sub-semiconductor-surface sample properties. On a GaAs/$Al_xGa_{1-x}As$ double barrier structure, e.g., it was possible to investigate the resonant states.[12] On self-assembled InAs quantum dots,[13–15] the BEEM current was found to be enhanced and fine structure in these BEEM spectra was attributed to the quantized states inside the dot.

In our group, the energetic distribution of ballistic electrons in GaAs was studied employing buried GaAs-$Al_xGa_{1-x}As$ resonant tunneling structures as an energy filter in BEEM experiments.[16,17] Due to the large difference in electron mass in the Au base electrode and the GaAs collector, we found that parallel momentum conservation leads to considerable electron refraction at the Au-GaAs interface and as a consequence, an almost linear behavior of the BEEM spectrum is observed in the energetic regime below the $Al_xGa_{1-x}As$ barrier height.

In the present work, we study ballistic electron transport through resonant tunneling structures, which are located directly below the metal base. On these samples, we observe a step-function-like behavior of the BEEM spectrum that is explained by a direct coupling of ballistic electrons in the Au base to the resonant level underneath. As a consequence of parallel momentum conservation and the large difference in electron mass between Au and GaAs, the resonant level now acts as a narrow filter both for wave vectors perpendicular ($k_{\perp}$) and parallel ($k_{\parallel}$) to the interface.

Two types of molecular beam epitaxy (MBE) grown resonant tunneling structures, double barrier resonant-tunneling diodes and GaAs-$Al_xGa_{1-x}As$ superlattices, were investigated. The double barrier structures were grown in the following way: On semi-insulating substrate, an *n*-doped GaAs collector region ($d=1\ \mu$m, $N_D=1\times10^{18}\,\mathrm{cm}^{-3}$) layer was grown, followed by a layer of 1500-Å undoped GaAs to provide a high sample resistance. On top of this layer, a double barrier resonant-tunneling diode and a very thin protecting GaAs cap layer was grown. On sample 1, the $Al_xGa_{1-x}As$ barriers had a thickness of 25 Å ($x=0.4$). The GaAs well between the barriers was 30 Å wide. Sample 2 had the same structure as sample 1, but slightly thicker $Al_xGa_{1-x}As$ barriers ($d=37$ Å). A plot of the self-consistently calculated[18] conduction-band profile is shown in Fig. 1(a). All samples were designed in such a way that just one resonant level exists within the $Al_xGa_{1-x}As$ barriers.

In addition to resonant-tunneling diodes, GaAs-AlGaAs superlattices were used in our experiment. Superlattice samples have the advantage that instead of a single resonant level, a miniband with a broad transmission range is formed

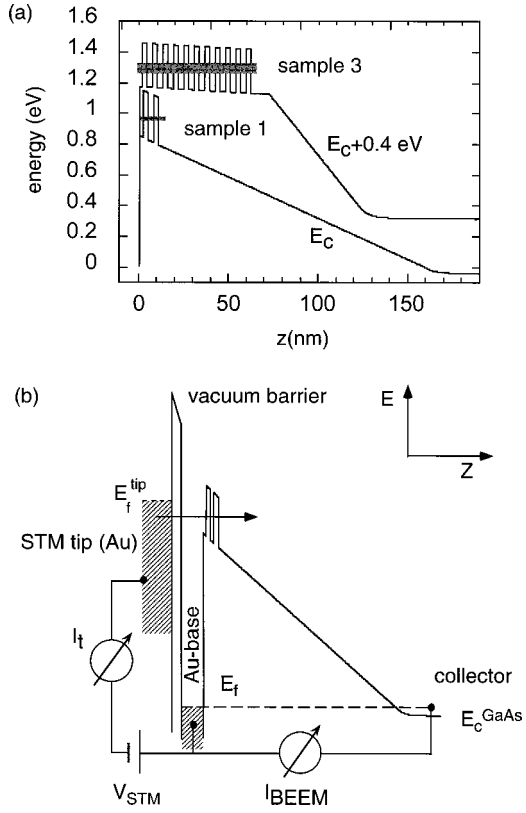

FIG. 1. (a) Self-consistently calculated conduction-band profiles of samples 1 and 3 ($T=100$ K). The resonant level of the double barrier structure and the miniband position of the superlattice are indicated by the gray bars. For better clarity, the band profile of sample 3 was shifted by 0.4 eV. (b) Schematical view of the experimental setup.

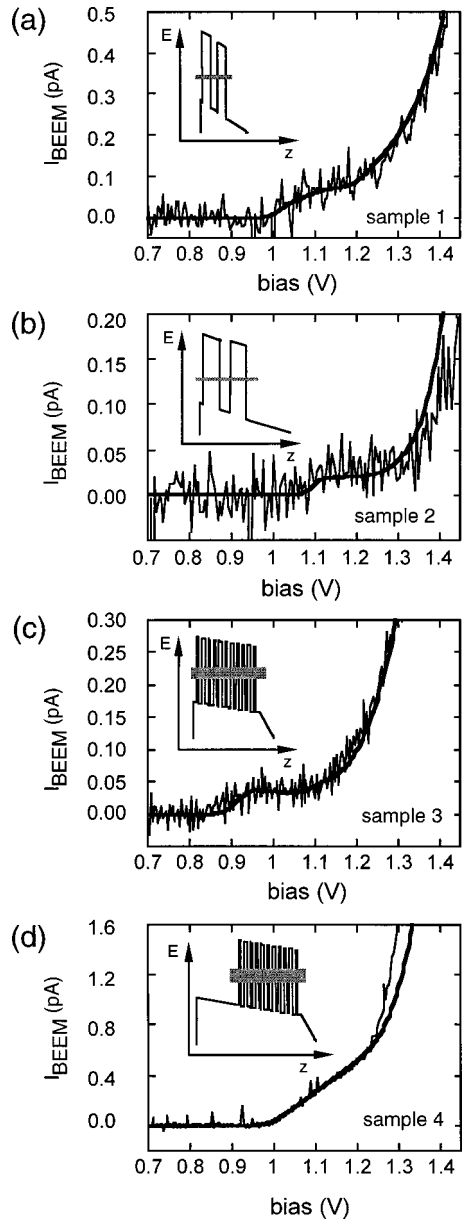

FIG. 2. (a)–(c) BEEM spectra of samples 1–3. The corresponding band profiles are shown in the inset. The thin lines are experimental data, the solid lines represent a fit to the data using a modified Bell-Kaiser model. (d) BEEM spectrum obtained on a reference sample with a superlattice buried 300 Å below the surface. All measurements were carried out at $T=100$ K and a tunneling current of 1 nA.

and at off-resonance conditions, all electrons are blocked off effectively due to the large total barrier width. Sample 3 was a 10 period 25-Å $(Al_{0.4}Ga_{0.6}As)$/30 Å (GaAs) MBE grown superlattice on top of 600-Å undoped GaAs and a highly doped *n*-type collector region. In this sample, the ''flatband'' condition necessary for the formation of a miniband in the superlattice was achieved by a *p*-type δ-doped layer ($N_A=1.4\times10^{13}\,\mathrm{cm}^{-2}$) between the superlattice and the highly doped collector region. The conduction-band profile of this sample is also shown in Fig. 1(a). For reference purposes, we also used the buried superlattices of our previous work,[16] which are identical to sample 3 besides an additional layer of GaAs ($d=300$ Å) on top of the superlattice (sample 4). The schematic band profiles of samples 2 and 4 are shown in the insets of Figs. 2(b) and 2(d).

To prepare the samples for BEEM, an In/Sn collector contact was first alloyed in forming gas atmosphere. Then, the samples were dipped into HCl to remove the native thin oxide layer. Finally an Au film (75 Å) was evaporated via a shadow mask. The size of the active area was $0.2\,\mathrm{mm}\times3\,\mathrm{mm}$. All measurements were carried out at a temperature of $T=100$ K to guarantee a high internal sample resistance, which is essential to prevent leakage currents and to obtain a good signal-to-noise ratio.

Figures 2(a)–2(d) show typical BEEM spectra measured on samples 1, 2, 3, and 4, respectively. Several features are evident: First, the spectra obtained on samples, where the resonant tunneling structure is directly below the metal base (a)–(c), are qualitatively different compared to the spectra obtained on the sample with a superlattice buried far below the metal base [Fig. 2(d)]. On the sample with a buried superlattice (sample 4), the BEEM spectrum is almost linear above the threshold voltage, which marks the energetic position, where the Fermi energy in the STM tip is aligned with the superlattice miniband. On samples 1–3, however, a steplike behavior is observed above the resonance position. The steplike behavior becomes more pronounced if the barriers of the resonant tunneling diode become thicker and is best pronounced on the superlattice (sample 3). Simultaneously, the step height decreases significantly from 4×10^{-13} Å

(sample 1) to 4×10^{-14} Å (sample 2). On the superlattice sample (sample 3), the step size is in the same order of magnitude as on sample 2.

To understand the qualitative difference between the BEEM spectra of samples 1–3 and sample 4, we first briefly review the processes that lead to the linear behavior of the BEEM spectrum of sample 4: If a ballistic electron crosses the Au-GaAs interface, its parallel momentum and its total energy has to be conserved, which means that $k_{\parallel}^{Au}=k_{\parallel}^{GaAs}$ and $E_{\perp}^{Au}+E_{\parallel}^{Au}=V_b+E_{\perp}^{GaAs}+E_{\parallel}^{GaAs}$. In this relation, $E_{\perp}=\hbar^2k_{\perp}^2/2m$ is the component of kinetic energy perpendicular to the interface and $E_{\parallel}=\hbar^2k_{\parallel}^2/2m$ the component of energy parallel to the interface. V_b is the Schottky barrier height at the Au-GaAs interface and the Fermi level in the Au base was defined to be zero. As the electron mass in GaAs is much smaller than in Au, an electron crossing the Au-GaAs interface will loose $E_{\perp}$ and gain $E_{\parallel}$ in GaAs according to $E_{\perp}^{GaAs}+V_b=E_{\perp}^{Au}-E_{\parallel}^{Au}(m_0/m^*-1)$, where m_0 is the free electron mass, and m^* the effective mass in GaAs. Although the total energy of the electron is conserved, this ''refraction'' behavior has a dramatic influence on the number of electrons that are transmitted through the buried superlattice. Through this refraction effect, electrons in the Au film at energies $E_{\perp}^{Au}$ totally off-resonance with the miniband, can now convert energy $E_{\perp}$ into $E_{\parallel}$ so that they are at resonance with the miniband position after they have crossed the interface. The total number of electrons that are transferred from higher values of $E_{\perp}^{Au}$ to lower values of $E_{\perp}^{GaAs}$ increases with increasing bias and finally leads to the linear behavior of the BEEM spectrum in the energy regime between the miniband and the top of the $Al_xGa_{1-x}As$ barriers.

On samples 1–3, the situation is different and here the electrons have to tunnel directly from the Au base through the $Al_xGa_{1-x}As$ barrier into the resonant level without being refracted beforehand in a layer of GaAs as on sample 4. As for the buried structure discussed above, parallel momentum conservation rules are also valid, but lead to different results. To clarify this, Fig. 3(a) shows the in-plane (parabolic) dispersion relations for electrons in the Au at different given values of $E_{\perp}^{Au}$ and the 2D-dispersion relation for electrons in GaAs at the resonance energy, respectively. Due to the large difference in effective mass, the curvature of the parabolas is strongly different. The bold part of the parabola indicates the $k_{\parallel}$ range of occupied states in the gold, the resonant state below the surface is empty. By changing the voltage V_{STM} between the STM tip and the Au base, the dispersion curves are shifted in energy. If V_{STM} is too small, the Au-dispersion curve is completely below the GaAs dispersion and therefore, tunneling into the GaAs is not possible. If V_{STM} increases, the Au parabola starts to intersect the GaAs parabola, which means that from the viewpoint of parallel momentum and total energy conservation, electrons are now allowed to tunnel as long as the intersection of both parabolas is in the range of occupied states. Note that this is an essential difference to the situation, where electrons tunnel between regions of identical effective mass: If the electron mass in the emitter and the resonant level is the same, tunneling is only possible if the incoming electrons and the resonant level are exactly aligned in $E_{\perp}$, but then, electrons of all possible $k_{\parallel}$ values are allowed to tunnel simultaneously.

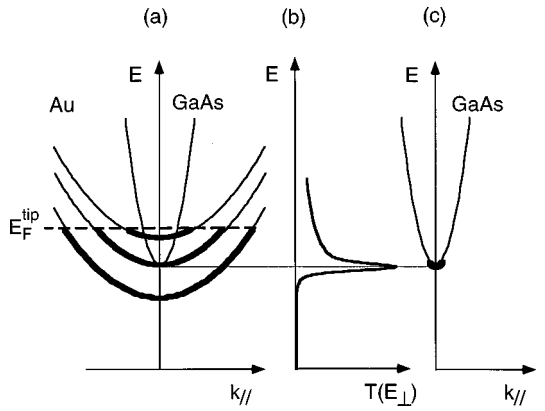

FIG. 3. (a) Dispersion relations $E(k)$ of electrons in Au and GaAs, respectively. The bold part of the parabola schematically indicates the $k_{\parallel}$ range of occupied states. V_{STM} is the bias between the STM tip and the Au base, E_F the Fermi energy in the tip. (b) Calculated transmission coefficient of sample 1. (c) Dispersion relation in GaAs and range of occupied states after transmission through the resonant tunneling structure. Due to the large difference in effective mass and the small resonance width, only electrons around $k_{\parallel}=0$ can be transmitted.

Besides total energy and parallel momentum conservation, however, also the transmission coefficient of the resonant tunneling structure $T(E_{\perp})$ has an influence on the $k_{\parallel}$ distribution of transmitted electrons. As one can see from the transmission coefficient plotted in Fig. 3(b), the resonant level acts as narrow energy filter in $E_{\perp}$ and suppresses all tunneling processes at higher energy, although they would be in principle allowed from the viewpoint of total energy and parallel momentum conservation. Moreover, due to the strongly different curvature of the dispersion curves in Au and GaAs [see Fig. 3(a)], only electrons around $k_{\parallel}=0$ are allowed to tunnel resonantly. This is illustrated in Fig. 3(c), where the narrow bold region of the parabola around $k_{\parallel}=0$ symbolizes the allowed $k_{\parallel}$ range of transmitted electrons in the GaAs.

As the resonant-tunneling structure acts as electron filter not only for $E_{\perp}$ but also in $k_{\parallel}$, this immediately explains the steplike features in the BEEM spectra: As long as the Fermi energy in the tip is below the $Al_xGa_{1-x}As$ barrier height, always a constant number of electrons will tunnel through the resonant level, since the allowed energy regime for resonant tunneling is always the same in $E_{\parallel}$ and $E_{\perp}$, independent of what the Fermi energy in the tip is.

In order to verify the these considerations quantitatively, we have calculated the BEEM spectra using a modified Bell-Kaiser model[6,7] where the transmission of the subsurface resonant states was taken into account.[19] As one can see from Fig. 2 and as demonstrated in our earlier work,[16] the model agrees excellently with the experimental data. For the buried superlattice [Fig. 2(d)], the linear behavior is nicely reproduced, which indicates that electron refraction effects at the Au-GaAs interface are the dominant mechanism on this sample. For bias voltages above $V_{STM}=1.25$ V, the fit deviates from the experimental data since the contributions of higher minibands in the superlattice and higher conduction bands in the GaAs were neglected in our calculation.

To calculate the spectra of samples 1–3, the $k_{\parallel}=0$ filtering effect was taken into account. Also in this case, excellent

agreement is achieved between the measured and calculated spectra. The steplike features become are more pronounced for sample 2 than for sample 1, which simply reflects the fact that for thicker barriers, the contribution of off-resonance currents is smaller. For the superlattice sample (sample 3), the steplike features are best resolved, since here the off-resonance current is totally blocked off by the large total barrier width in the superlattice. It should be mentioned that the current due to ballistic electron tunneling directly through the subsurface resonant level is quite small. This, however, is not astonishing, since due to the $k_{\|}=0$ filtering effect only a small amount of electrons can be transmitted through the resonant state of the resonant double barrier structure or the superlattice miniband, respectively. As our simulations have shown, the step height in the BEEM spectrum depends on the width of the $k_{\|}$ filter. According to our simulation, the calculated BEEM current is much too small, if only electrons at exactly $k_{\|}=0$ are taken into account. Integrating over a kT ($T=100$ K) wide energy range in $E_{\|}$, however, a good agreement between the calculated and measured spectra is achieved.

From the above considerations, two major conclusions can be drawn: First, resonant tunneling structures directly below the surface act as narrow $k_{\perp}$ and $k_{\|}=0$ filter, which means that one can expect an enhanced spatial resolution for BEEM on buried structures due to the strongly directed beam of ballistic electrons injected into the semiconductor. The actual spatial resolution will depend on the applied bias and other various parameters, but as an example, let us consider the situation at a bias of 1.1 V, where the Fermi level in the tip is just aligned with the resonant level in sample 2, an Au-GaAs Schottky barrier height of 0.9 eV, a base thickness of 75 Å and a depth of 300 Å below the Au-GaAs interface. For these parameters, one can estimate a radius of $r\approx 8$ Å for the acceptance cone at the Au-GaAs interface, which, due to electron refraction, increases up to $r\approx 140$ Å at a depth 300 Å below the surface. Using a $k_{\|}$ filter having a width of kT ($T=100$ K), however, the expected radius of the ballistic electron beam has only a size of $r\approx 30$ Å. Experiments to determine the actual resolution on samples with a $k_{\|}$ filter will be the subject of further investigations.

As a second major conclusion we want to emphasize that the above considerations can be applied to device applications. As already mentioned in the Introduction, electron refraction effects have a major influence in the InAs-AlSb tunneling structures, where the difference in effective mass between both materials is also large. On properly designed samples, one could use the mass difference to perform experiments in ''electron optics'' in analogy to classical optics experiments, which are based on the difference in refractive index between two materials. Even BEEM experiments can be ported to devices. By replacing the scanning tunneling microscope by a metal-oxide-metal (Al-Al_2O_3-Al) tunneling junction on top of a GaAs-$Al_xGa_{1-x}As$ resonant tunneling structure, e.g., one should obtain a ballistic electron beam having a narrow energetic distribution both in $E_{\|}$ and $E_{\perp}$. Depending on the area of the tunneling contact, large ballistic currents can be expected, which opens possibilities for a whole field of new experiments on a new class of samples.

In summary, electron transport between materials of different effective mass and different dimensionality was investigated by BEEM. It was shown that for electrons tunneling from an area of high effective mass through a resonant level in an area of low effective mass, a momentum filter is established for $k_{\|}=0$. As a consequence, only a highly directed beam of ballistic electrons is transmitted through these structures and a strongly enhanced spatial and energetic resolution for BEEM on buried structures is expected. The experiment also demonstrates that in analogy to classical optics, electron transfer between regions of different effective mass can be treated the same way as a beam of light at the interface between two materials of different refractive index. The underlying physical principle also applies for all devices using layered structures with large a difference in effective mass, such as the InAs-AlSb material system.

This work was sponsored by FWF Project No. P12925-TPH and Gesellschaft für Mikroelektronik (GMe). The authors are grateful to E. Gornik for continuous support.

*Electronic address: juergen.smoliner@tuwien.ac.at

[1] T. B. Boykin, Phys. Rev. B **51**, 4289 (1995).
[2] Xue-Hua Wang, Ben-Juan Gu, and Guo-Zhen Yang, Phys. Rev. B **55**, 9340 (1997).
[3] J. N. Schulman, Appl. Phys. Lett. **72**, 2829 (1998).
[4] V. V. Paranjape, Phys. Rev. B **52**, 10 740 (1995).
[5] R. Tsu and L. Esaki, Appl. Phys. Lett. **22**, 562 (1973).
[6] W. J. Kaiser and L. D. Bell, Phys. Rev. Lett. **60**, 1406 (1988).
[7] L. D. Bell and W. J. Kaiser, Phys. Rev. Lett. **61**, 2368 (1988).
[8] W. J. Kaiser, M. H. Hecht, L. D. Bell, F. J. Grunthaner, J. J. Liu, and L. C. Davis, Phys. Rev. B **48**, 18 324 (1993).
[9] H. Sirringhaus, E. Y. Lee, and H. von Känel, Phys. Rev. Lett. **73**, 577 (1994).
[10] R. Ludeke, M. Prietsch, and A. Samsavar, J. Vac. Sci. Technol. B **9**, 2342 (1991).
[11] M. Prietsch and R. Ludeke, Phys. Rev. Lett. **66**, 2511 (1991).
[12] T. Sajoto, J. J. O'Shea, S. Bhargava, D. Leonard, M. A. Chin, and V. Narayanamurti, Phys. Rev. Lett. **74**, 3427 (1995).
[13] M. E. Rubin, G. Medeiros-Ribeiro, J. J. O'Shea, M. A. Chin, E. Y. Lee, P. M. Petroff, and V. Narayanamurti, Phys. Rev. Lett. **77**, 5268 (1996).
[14] W. Wu, J. R. Tucker, G. S. Solomon, and J. S. Harris, Jr., Appl. Phys. Lett. **71**, 1083 (1997).
[15] E. Y. Lee, V. Narayanamurti, and D. L. Smith, Phys. Rev. B **55**, R16 033 (1997).
[16] J. Smoliner, R. Heer, C. Eder, and G. Strasser, Phys. Rev. B **58**, 7516 (1998).
[17] R. Heer, J. Smoliner, G. Strasser, and E. Gornik, Appl. Phys. Lett. **73**, 1218 (1998).
[18] Poisson solver by Greg Snider, Department of Electrical Engineering, University of Notre Dame, Notre Dame, IN 46556. Electronic address: snider.7@nd.edu
[19] D. L. Smith and Sh. M. Kogan, Phys. Rev. B **54**, 10 354 (1996).